ELSEVIER

Journal of Nuclear Materials 280 (2000) 255–263

journal of nuclear materials

www.elsevier.nl/locate/jnucmat

Ultrashort X-ray pulse generation using subpicosecond electron linac

Hideki Harano *, Kenichi Kinoshita, Koji Yoshii, Toru Ueda, Shunsuke Okita, Mitsuru Uesaka

Nuclear Engineering Research Laboratory, University of Tokyo, 2-22 Shirakata-shirane Tokai-mura, Naka-gun, Ibaraki 319-1106, Japan

Received 2 February 2000; accepted 5 May 2000

Abstract

As a promising tool for ultrafast material analyses, we propose to utilize the X-ray pulse which may be generated in a quite simple manner using subpicosecond electron linacs. The properties of the X-ray were numerically studied with the EGS4 code. Verification of the X-ray generation was also conducted at the Nuclear Engineering Research Laboratory (NERL) linac and clear diffraction patterns of characteristic X-ray were obtained for typical single crystals.

PACS: 31.70.Hq; 61.10.−i; 78.47.+p; 82.40.Js

1. Introduction

Recent remarkable progress in ultrashort pulse generation technology has brought entirely new possibilities not only to realize the dynamic analyses in material property research having been performed in static manners so far, but also to provide the direct observation of ultrafast unknown phenomena with the time resolution of better than 1 ps. Using mode-locked lasers, the femtosecond evolution of electronic states in solid- and photo-initiated chemical reactions has been examined by laser pump and probe spectroscopy and laser flash photolysis. On the other hand, the temporal changes of atomic arrangement have been observed mainly with by synchrotron X-rays with the time resolution longer than picosecond [1–3]. Recent developments in high-power laser technology such as a table-top tera watt laser have permitted the generation of pico- to subpico-second X-ray pulses. Energy-tunable sharply-directed X-ray pulses were produced by the Thomson scattering of ultrashort laser pulses synchronized to relativistic electron beams [4–7]. Laboratory-scale sources of intense ultrashort X-ray pulses are accessible by focusing an intense laser on solid targets [8–12]. The latter X-ray, known as the laser-produced plasma X-ray (LPX), has been applied to observe ultrafast evolving diffraction patterns for organic films [10] and semiconductor crystals [12] irradiated by ultrashort laser pulses. It is expected that appropriate selection of the pump pulse allows the further treatment of various ultrafast phenomena such as lattice vibration (phonon oscillation) and phase transition, which may result in experimental verification for the solid-state theoretical physics and molecular dynamics calculation.

Ultrashort electron pulses have been one of the indispensable diagnostic tools for probing radiation-induced chemical reactions. Now the electron pulses shorter than picosecond are available by linear accelerators (linac) [13–16]. We have two types of S-band linac at the Nuclear Engineering Research Laboratory (NERL) and both of them are capable of producing subpicosecond single-bunch pulses by magnetic pulse compression. Precise pulse-width measurement has been carried out using a femtosecond streak camera [17] and coherent far-infrared transition radiation interferometry [18,19]. The first linac generates 35 MeV electrons and

* Corresponding author. Tel.: +81-29 287 8473; fax: +81-29 287 8471.

E-mail address: harano@tokai.t.u-tokyo.ac.jp (H. Harano).

0022-3115/00/$ - see front matter
PII: S0022-3115(00)00067-2

uses an achromatic-arc-type magnetic compressor [13]. In the second linac, the photocathode RF gun [20] is installed with a chicane-type magnetic compressor and 18 MeV electrons are available [18]. These linacs can also operate synchronized with external systems in less than 4 ps time resolution [21]. Several experiments such as pulse radiolysis for radiation chemistry [22], laser wakefield acceleration [23], Thomson scattered X-ray generation [24] were performed using the synchronized pulses from linac and T^3 laser. The X-band linac system is planned to be introduced in future, which is evaluated to produce 30 MeV electron pulses of 100 fs duration [25].

In this study, we propose a quite simple method of the ultrashort X-ray pulse generation only by irradiating the linac-produced subpicosecond electron pulses on solid targets. This technique does not need any severe synchronization system which is necessary for the Thomson scattering X-ray production [21]. A wide variety of subpicosecond pump and probe experiments are expected to be performed by employing the resulted X-ray, abbreviated as LINAX (LINAc-based X-ray) here, as a probe pulse, and the electron itself or various converted radiations in the range of infrared rays to millimeter waves like a transition radiation as a pump pulse. In the subpicosecond analysis, it is desirable to produce both pump and probe pulses from the same electron pulse so as to avoid the timing jitter problem in adding up accumulated results. The properties of the X-ray have been totally examined numerically by using the general-purpose Monte-Carlo electron–photon transport code EGS4 [26]. We also report the experiments to generate the X-rays and to obtain their diffraction images for several typical single crystals performed with the NERL linac.

2. Properties of linac-based X-ray

Electrons of the order of 10 MeV impinging upon a solid target experience multiple Coulomb scattering and sometimes emit Bremsstrahlung photons influenced by the electric field of the surrounding nuclei while being transported. Electron–positron pairs are produced by the photons more energetic than 1.02 MeV inside the target. The positrons are decelerated and annihilated with creating pairs of 0.511 MeV γ-ray instead. The photons lose some of their energy by Compton scattering with the outer-shell electrons of the constituent atoms, and are absorbed and converted into characteristic X-rays through photoelectric effect. The direct collision between the incident and the inner-shell electron also results in the characteristic X-ray production. It is beyond the scope of this paper to discuss the further details of the physical mechanism here (see for example [27]). In this section, the above processes known as the electromagnetic cascade were simulated as precisely as possible and the characteristics of the photon LINAX was examined using the EGS4 electron–photon transport Monte-Carlo code system [26]. The PRESTA algorithm [28] was utilized for the optimum treatment of the transport of low-energy electron. The improved sampling of Bremsstrahlung angular distribution [29] was employed. Particle splitting was also applied to Bremsstrahlung generation for enhancement of the calculation efficiency.

2.1. Energy spectra

Fig. 1(a) shows the energy spectra of the LINAX emitted behind copper sheets of different thicknesses, where the pencil-like (zero transverse width) electron beam with a monoenergy of 35 MeV is incident perpendicularly on the surface. The subpicosecond electron pulses of this energy are produced by the first linac at NERL. An eminent peak of characteristic K-X-rays is observed around 8 keV over the mainly Bremsstrahlung-originated portion continuously spread out toward the initial energy of electron.

The differences in shape between the continuous spectra seen in Fig. 1(a) are explicable as follows by comparison of the copper thickness t with the attenuation length λ defined as an e-folding length of X-ray flux inside matter. The slight damping just below the maximum energy is observed apparently for the 10-mm thick case due to the energy decay of the electron. Except for this, the spectra above 300 keV are similar with the intensity proportional to the thickness, where $\lambda \gg 10$ mm, i.e. the absorption of the X-ray by the sheet itself is negligible. For the range from 300 down to 13 keV where $\lambda > 10$ μm and < 10 mm, the spectra widely vary depending on the thickness, because of the large self-absorption effect on the X-rays which have the attenuation length shorter than the sheet thickness. Due to the enhancement of photo-absorption cross-section, all the spectra exhibit a noticeable drop in intensity just above the K-edge. The spectra below 13 keV appear to be quite similar in both shape and intensity, since the strong self absorption allows the contribution of X-rays only generated at the surface layer in this energy region.

The yields of characteristic K-X-rays are roughly comparable for the cases of thickness more than 100 μm since the attenuation length of the K-X-ray is about 22 μm. The K-X-rays are generated through deexcitaion of the K-shell hole which is produced through two channels: K-shell photoionization (PI) and electron-impact ionization (EII). The channel PI is a double-step process triggered by the secondary-emitted particles – the Bremsstrahlung photons created by the incident electrons, whereas EII is a single-step process caused by the bombardment of the incident electron itself with the K-shell electron. The EII process is not treated in the default EGS4 code so the modified version of the EGS4

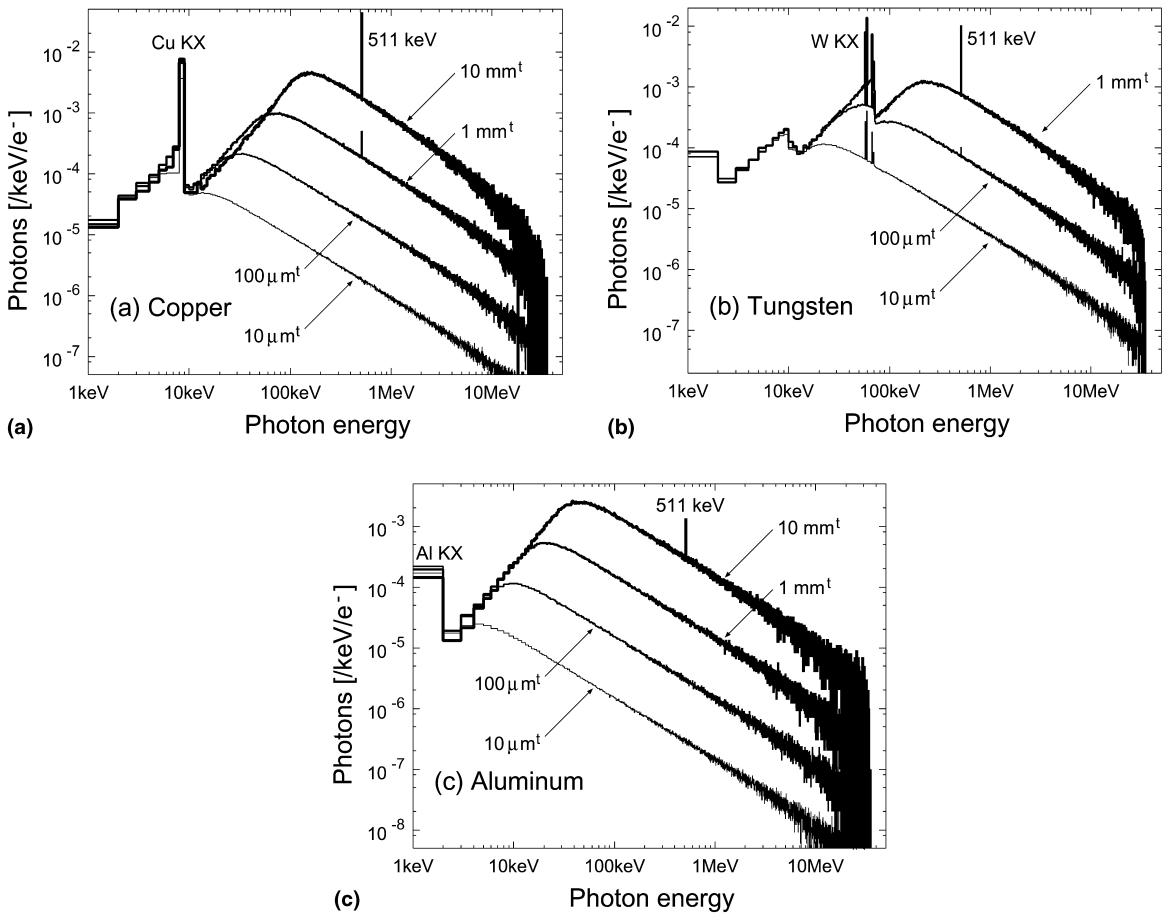

Fig. 1. Energy spectra of the X-rays emerged from sheet targets for the normal injection of 35 MeV electrons. The sheet thickness are indicated: (a) copper; (b) tungsten; (c) aluminum.

code is utilized here which Namito et al. [30] have developed to deal with the K-shell EII. The adopted EII cross-section is derived by Casnati [31] and corrected to include a relativisity. The K-X-rays are produced dominantly via EII in all calculations. The PI fraction is increased with the thickness, reaching up to 10% for the 10-mm thick case. This fact indicates that for the thin case only single-step processes should be considered, however, the multi-step processes become also important for the thick case. Only for the cases thicker than 1 mm, the 511 keV peaks are observed, which consist of the annihilation γ-rays produced after the triple sequential processes of the Bremsstrahlung, the pair creation and the positron annihilation.

We also calculated the case for the incidence of the 18 MeV electrons of which the subpicosecond pulses are available from the second linac at the NERL. The energy spectra are equal to those of the 35 MeV case except for the difference in the maximum energy of the continuous X-rays and for the slight decrease of the K-X-ray yield of less than 10% due to the energy dependence of the EII reactivity [30].

As seen in Fig. 1(b), energy spectra were also obtained for the sheets of tungsten having the 74th atomic number larger than the 29th of that of copper. K-X-rays, continuous Bremsstrahlung X-rays and annihilation γ-rays were observed which are mainly governed by the principles explained above. The L-X-ray generation is not taken into account in these calculations. The radiation length of tungsten is 6.4 g/cm^2 (0.33 cm) and about half as much as copper's 12.9 g/cm^2 (1.44 cm), where the radiation length is an e-folding length of electron energy attenuation due to Bremsstrahlung. So the intensity of the continuous X-rays is much higher than the copper case. The K-X-ray yield increases with the thickness since it has a relatively long attenuation length of about 130 μm. Although the EII cross-section decreases with increasing atomic number, the K-X-ray yield exceeds that of the copper case for the converter thicker than 1 mm, where the PI fraction goes

up to over 80%. The large effective thickness of tungsten for the Bremsstrahlung generation enhances the subsequent PI process which has a larger cross-section for high atomic number materials. The spectrum for the 1-cm thick case is not shown in the figure, where the incident electrons stop inside the sheet since the path range of 35 MeV electron in tungsten is about half of that of the thickness. Fig. 1(c) indicates the energy spectra for the sheets of aluminum having the 13th atomic number. The peak intensity of the K-X-rays were however much reduced since the K-shell hole is stabilized mainly by the Auger relaxation process resulting in the suppression of K-X-ray generation for lower atomic number materials.

2.2. Angular distributions

Fig. 2 depicts the X-ray emission profiles on the downstream side of the copper-sheet converters of different thickness, as the function of the emitted angle with respect to the incident electron direction. The distributions are found to be sharpened straight forward, typically seen in angular profiles of Bremsstrahlung generation. The peak becomes more broadened consistently with the thickness since the initiating electrons are subjected to the direction changes due to the multiple scattering. On the other hand, the characteristic K-X-ray emission profiles appear to be isotropic. These strong angular dependence are also observed for other materials such as aluminum and tungsten. For the experiments having a particular interest on the characteristic X-ray, we should make use of the X-rays emitted off the incident electron beam line in order to achieve high S/N ratios. Fig. 3 shows the calculated spectra of forward-emitted and backward-emitted X-rays from the 100-μm thick copper sheet, for comparison. The K-X-ray yields are nearly equal, while the intensity of the continuous X-rays, mainly due to the Bremsstrahlung, of the backward emission is much smaller than that of the forward emission by a factor of several hundreds to thousands. For the utilization of the X-ray other than the forward emission, however, special attention should be given to the pulse duration expansion due to the geometrical factor explained below.

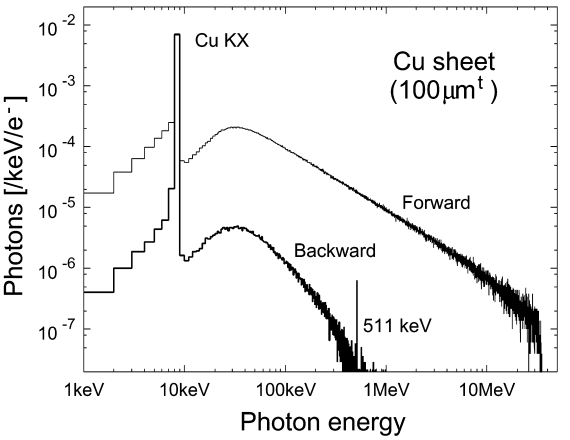

Fig. 3. Comparison of the energy spectra between the forward-emitted and the backward-emitted X-rays from a 100-μm thick copper sheet.

2.3. Pulse shapes

The pulse shapes of the X-ray were also calculated by adding up the transit time of the every transport step in

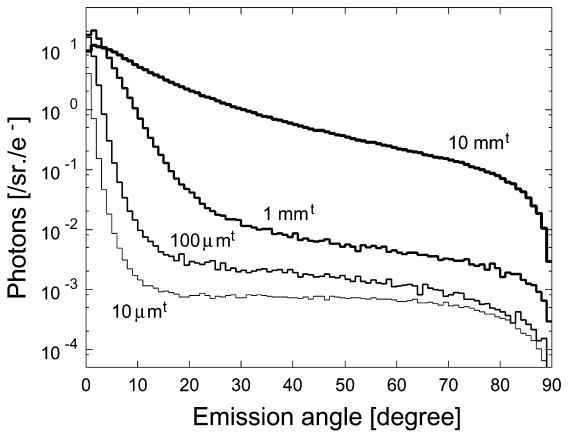

Fig. 2. Angular distributions of the X-rays on the downstream side of copper sheets for the normal injection of 35 MeV electrons. The angle shown on the bottom axis is measured from the incident-beam direction.

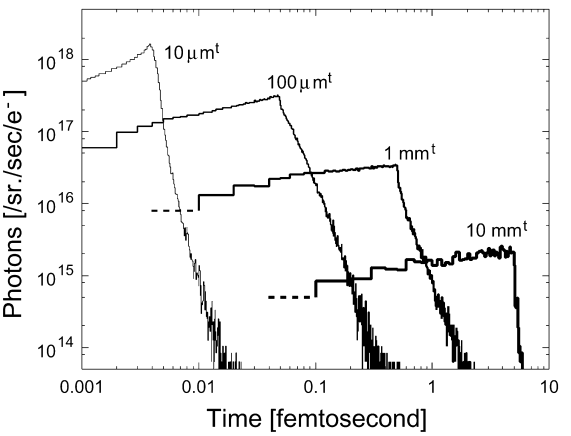

Fig. 4. Pulse shapes of the forward-emitted X-rays from copper sheets of various thickness for the normal injection of 35 MeV electrons.

the EGS4 user code. Fig. 4 shows the temporal evolution of the brightness of the X-rays emitted straight forward from the copper sheets. The incident electron pulse duration was regarded as zero. So the actual X-ray pulse shapes may be derived by convoluting the resultant impulse responses with the incident electron pulse shape, introduced in [13,18] for the NERL linacs. As the increase of the thickness, the obtained pulse duration was elongated gradually, which is still much shorter than that of the actual electron pulses, that is, subpicosecond. This slight elongation is mainly due to the distortion of the trajectory of initiating electron resulting from the lateral deflection by multiple scattering. The pulse shapes and durations of the forward-emitted characteristic K-X-ray were roughly identical to those shown in Fig. 4. The hole in the K-shell has an ultrashort lifetime of about 1 fs [32], which was disregarded in the calculations so that the K-X-ray was emitted immediately after the K-shell ionization. For the tungsten- and aluminum-sheet converters, the pulse shapes were similar to those shown in Fig. 4, while the pulse durations were at the most 10% longer and shorter, respectively, than those from the copper sheet of the same thickness. It should be noted that the X-ray pulse of the non-forward emission undergoes severe pulse expansion due to a geometrical factor since there is a certain time lag of the X-ray generation at upstream and downstream caused by the finite light speed. The light travels 300 μm per 1 ps. This time lag will be cancelled for the forward-emitted X-rays if the electron energy is relativistic.

2.4. Applications

In this section, we have totally characterized the LINAX pulses numerically and clarified their governing parameters. The LINAX mainly consists of the continuous X-rays emitted sharply straight forward and the characteristic X-rays emitted isotropically with the subpicosecond pulse duration almost keeping that of incident electron pulses. The features such as spectrum, intensity, angular distribution and pulse duration are strongly dependent on the material and size of the converter as described above. The NERL linacs typically generate the electron pulses with the electric charge of 1 nC ($\sim 6.25 \times 10^9$ electrons) and with the finite diameter of 10 mm. For the operation at the repetition rate of 10 Hz, the parallel beam of the continuous X-rays is generated with the average flux of the order of 10^{10} photons/mm^2/s and the characteristic X-rays emit isotropically with the average intensity of 10^7–10^8 photons/sr/s.

These unique properties of the LINAX will permit various applications. The high energy part of the continuous X-rays is rather useful as a pump pulse for the elucidation of the most initial process of γ-ray induced radiation damage, for instance. Use of electron-produced infrared radiations as a probe pulse allows the subpicosecond pump and probe analysis for the formation of defects such as a color center which can be observed by infrared spectroscopy. The sharply forward-directed emission of the continuous X-rays can be also applied to a Laue diffraction method, as illustrated in Fig. 5, to monitor the ultrafast time-dependent structural changes in single crystals.

For the use of the characteristic X-rays, the non-forward emission from the thin target scaled by their attenuation length should be utilized with the attention to the elongation of pulse duration due to the geometrical factor. It is possible to compensate the emission time difference to some extent by employing a tiny converter or by locating a pinhole between the converter and the sample. Fig. 6 depicts an example of the configuration with the pinhole, where we can execute experiments analogous to that having been performed in [12]. Similarly, the continuous X-rays non-forwardly emitted from the comparatively thick target can be used for the ultrafast time-dependent

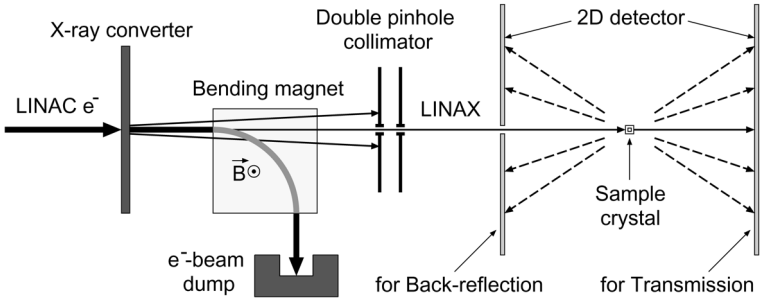

Fig. 5. Scheme of a Laue diffraction method using the continuous component of the forward-emitted X-rays. The configurations of transmission and of back-reflection are shown. Collimation of the beam with double pinholes forms Laue spots on 2-D detectors such as photographic films and imaging plates, which gives the orientation of the diffracting planes and the information to determine the crystal structure.

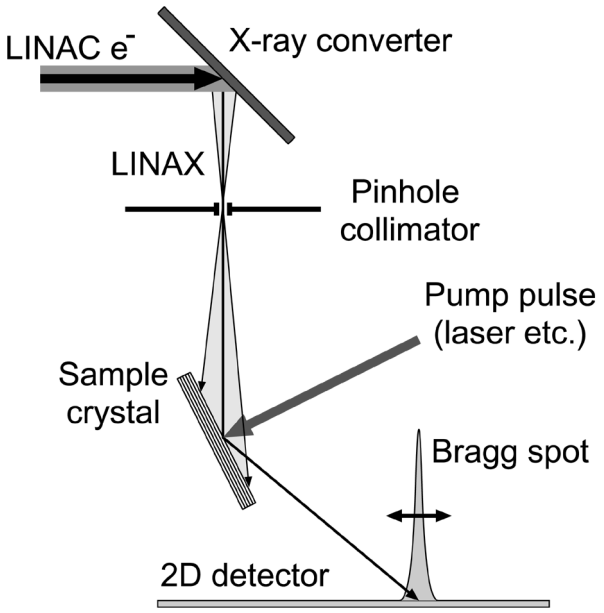

Fig. 6. Scheme of a Bragg diffraction method using the characteristic X-rays diverging from a pinhole. The diffracted patterns are comprised of the X-ray incident on the sample crystal only with Bragg angle. These patterns move depending on the change in lattice spacing of the sample or sometimes vanish due to structural transitions.

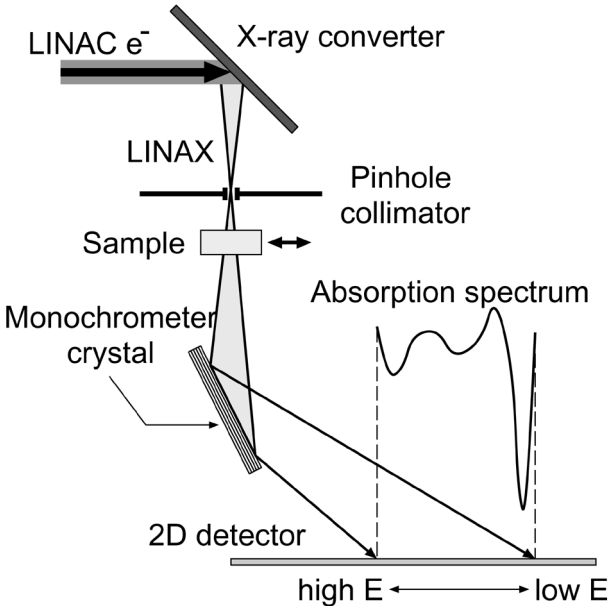

Fig. 7. Scheme of the X-ray absorption measurements using the continuous component of the diverging X-rays from a pinhole. The absorption spectrum is obtained from the difference in the X-ray intensity profile on the 2-D detector between that with and without the sample.

measurement of X-ray absorption such as that of an extended X-ray absorption fine structure (EXAFS) in the manner shown in Fig. 7. The absorption spectrum is obtained from the difference in the X-ray intensity profile on the two-dimensional detector between that with and without the sample. Further detailed feasibility investigations of the LINAX remain as a future work.

3. Experiments

The LINAX generation and its experimental verification by X-ray diffraction were executed using the NERL linac, based on the above information obtained from the EGS4 simulations. As shown in Fig. 8, the LINAX pulses are created from the X-ray converter irradiated by the linac-produced electron beam. For easy alignment, large wafers or disks of single crystals are employed as the samples for X-ray diffraction and mounted on a goniometer. The two-dimensional diffraction images are taken by X-ray imaging plates (BAS-SR, Fuji Photo Film) with a spatial resolution of 50 μm. The samples and the imaging plates are installed inside the lead box for the shielding of the background γ-rays scattered from surrounding materials. The X-rays may reach the sample surface only through the 5-mm width slit provided in the . Polyethylene blocks are also located so as to shield the photoneutron as indicated in Fig. 8. Although the imaging plate is not inherently sensitive to neutrons, this shielding contributes to the reduction of background level on the plate. This reason may be that the photoneutrons absorbed in the lead shielding produce capture γ-rays. The linac operated without the magnetic pulse compression and produced 35 MeV electron pulses with an electric charge of about 1 nC.

Fig. 9 depicts the diffraction image for a silicon wafer of (1 1 1) orientation. A 15-μm thick copper foil was utilized for the X-ray converter. There are three types of spots observed on the image, viz., the spot exposed directly to the X-ray passing through the slit, the shadow cast by the sample, and the Bragg spot composed of the diffracted copper K-X-rays appearing only when the Bragg condition being satisfied. The required irradiation time was about 20 min at a 10 Hz operation – corresponding to the accumulation over 10^4 pulses. By adopting the copper foils in piles as the X-ray converter, we studied the effect of the converter thickness on the diffraction image. As the thickness is increased, the Bragg spot decreases its prominence due to the elevation of the background level, which was consistent with the EGS4 calculations.

The diffraction images were also obtained for the disk samples of GaAs(1 1 1), Ge(1 1 1), NaCl(2 0 0), KCl(2 0 0), BaF_2(1 1 1), CaF_2(2 2 0), and other typical single crystals with the orientation face permitting strong diffraction. All the crystals used here are easily available and tractable with little deliquescence. The samples consisting of heavier atoms showed higher reflectivity among those with the same crystal structure and diffracting plane; the Bragg spot for the Ge and GaAs appeared to be a few times as brighter as that for the Si, for instance. This tendency may be attributed to the difference in atomic-number dependence of the cross-section between Thomson scattering and photo absorption. By the use of the copper wire 100 μm in diameter, two fine lines, respectively consisting of diffracted $K\alpha_1$ (1.5405 Å) and $K\alpha_2$ (1.5443 Å) were clearly resolved for the semiconductor wafers on the imaging plate, as shown in Fig. 10. This situation corresponds to the case where the tiny X-ray converter is employed instead of the pinhole collimator in Fig. 6. The irradiation time was several times more than that required for the foil converter. For the samples of ionic crystal,

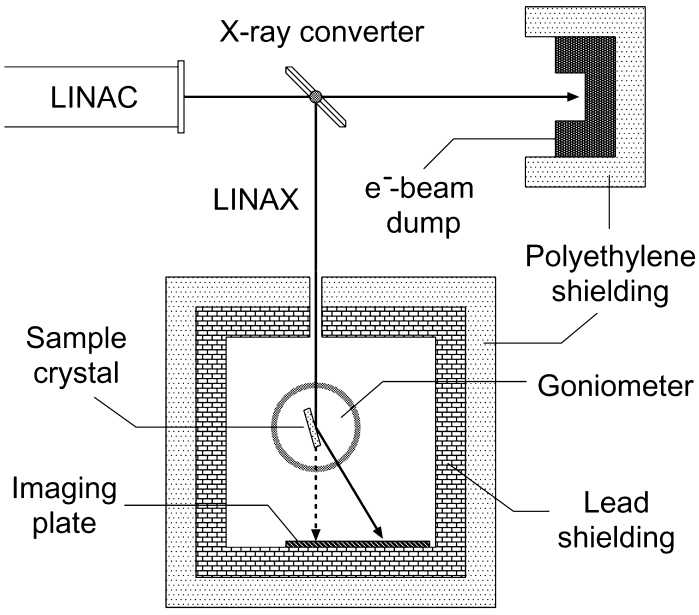

Fig. 8. Experimental configuration of the LINAX-generation experiment using the NERL linac.

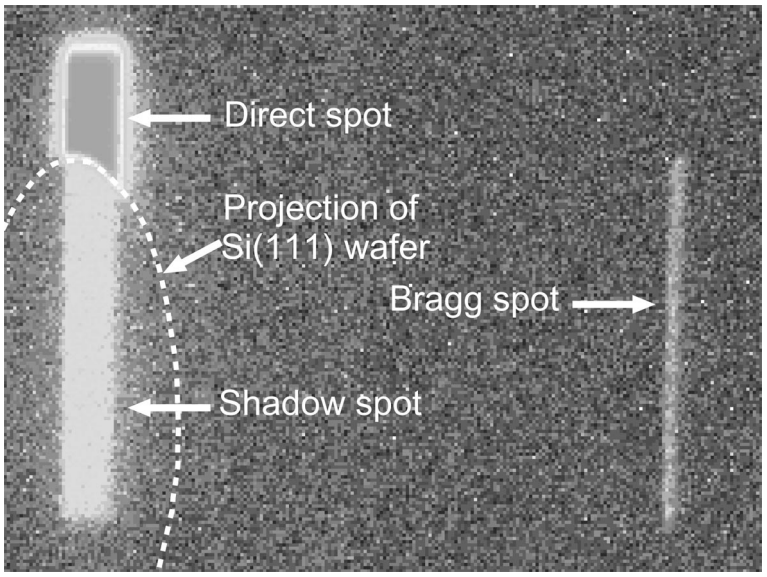

Fig. 9. X-ray diffraction image for a Si(1 1 1)-wafer sample using a 15-μm thick copper-foil converter.

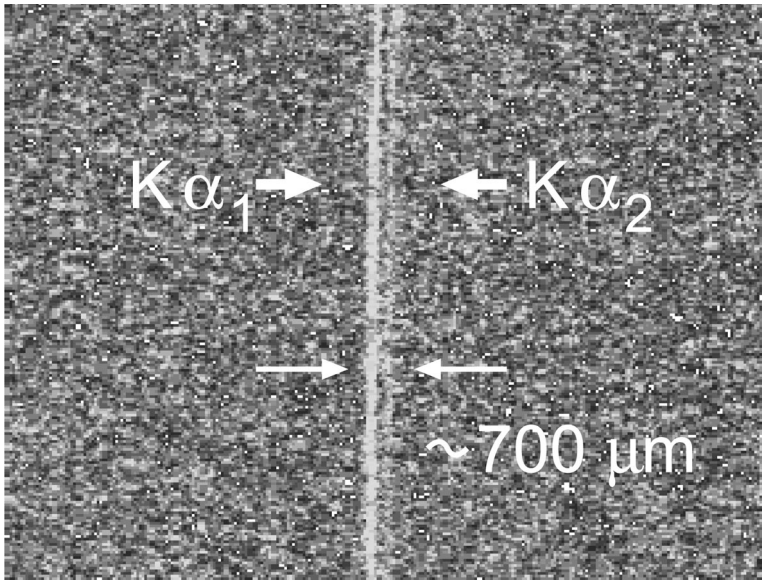

Fig. 10. Two clearly resolved Bragg lines of copper $K\alpha_1$ and $K\alpha_2$ by the use of a copper-wire converter 100 μm in diameter for Si(1 1 1) wafer sample.

their large mosaicity blurred each line and disturbed separation.

4. Summary

The simple method of ultrashort X-ray pulse generation with use made of subpicosecond electron linac was proposed. The detailed properties of this unique X-ray were numerically clarified with the EGS4 code. Generation of the X-ray was confirmed experimentally, using the NERL linac and the diffraction images of copper K-X-ray were obtained for the typical single crystals. Further characterization of the X-ray is in progress with the novel instruments like an X-ray streak camera. Feasibility study of the X-ray to various dynamic analyses is also currently under way. As a next stage, we plan to perform time-resolved X-ray diffraction experi-

ments to observe the heat expansion of semiconductor crystals by the combination between the NERL linac and the T^3 laser synchronized within a few picosecond.

Acknowledgements

The authors are thankful to Dr Namito of the High Energy Accelerator Research Organization for his help in using the EGS4 code. They also thank Dr Niimura of the Japan Atomic Energy Research Institute and Dr Yoneoka of the University of Tokyo for valuable suggestion on the X-ray diffraction experiment.

References

[1] B.C. Larson, J.Z. Tischler, D. Mills, J. Mater. Res. 1 (1986) 144.
[2] S. Kojima, Y. Kudo, S. Kawado, T. Ishikawa, T. Matsushita, Rev. Sci. Instrum. 66 (1995) 1419.
[3] J. Larsson, A.M. Lindenberg, P.J. Schuck, R.W. Falcone, P.A. Heimann, H.A. Padmore, P.H. Bucksbaum, R.W. Lee, J.S. Wark, Appl. Phys. A 66 (1998) 587.
[4] R.W. Schoenlein, W.P. Leemans, A.H. Chin, P. Volfbeyn, T.E. Glover, P. Balling, M. Zolotorev, K.-J. Kim, S. Chattopadhyay, C.V. Shank, Science 274 (1996) 236.
[5] W.P. Leemans, R.W. Schoenlein, P. Volfbeyn, A.H. Chin, T.E. Glover, P. Balling, M. Zolotorev, K.-J. Kim, S. Chattopadhyay, C.V. Shank, IEEE J. Quantum Electron. 33 (1997) 1925.
[6] K.-J. Kim, S. Chattopadhyay, C.V. Shank, Nucl. Instrum. and Meth. A 341 (1994) 351.
[7] E. Esarey, P. Sprangle, A. Ting, S.K. Ride, Nucl. Instrum. and Meth. A 331 (1993) 545.
[8] J.D. Kmetec, C.L. Gordon III, J.J. Macklin, B.E. Lemoff, G.S. Brown, S.E. Harris, Phys. Rev. Lett. 68 (1992) 1527.
[9] A. Rousse, P. Audebert, J.P. Geindre, F. Fallies, J.C. Gauthier, A. Mysyrowicz, G. Grillon, A. Antonetti, Phys. Rev. E 50 (1994) 2200.
[10] C. Rischel, A. Rousse, I. Uschmann, P.-A. Albouy, J.-P. Geindre, P. Audebert, J.-C. Gauthier, E. Förster, J.-L. Martin, A. Antonetti, Nature 390 (1997) 490.
[11] M. Yoshida, Y. Fujimoto, Y. Hironaka, K.G. Nakamura, K. Kondo, M. Ohtani, H. Tsunemi, Appl. Phys. Lett. 73 (1998) 1.
[12] C. Rose-Petruck, R. Jimenez, T. Guo, A. Cavalleri, C.W. Siders, F. Ráksi, J.A. Squier, B.C. Walker, K.R. Wilson, C.P. Barty, Nature 398 (1999) 310.
[13] M. Uesaka, K. Tauchi, T. Kozawa, T. Kobayashi, T. Ueda, K. Miya, Phys. Rev. E 50 (1994) 3068.
[14] P. Kung, H. Lihn, H. Wiedemann, Phys. Rev. Lett. 73 (1994) 967.
[15] B.E. Carlsten, S.J. Russell, Phys. Rev. E 53 (1996) 2072.
[16] X.J. Wang, X. Qiu, I. BenZvi, Phys. Rev. E 54 (1996) 3121.
[17] M. Uesaka, T. Ueda, T. Kozawa, T. Kobayashi, Nucl. Instrum. and Meth. A 406 (1998) 371.
[18] M. Uesaka, K. Kinoshita, T. Watanabe, T. Ueda, K. Yoshii, H. Harano, K. Nakajima, A. Ogata, F. Sakai, H. Kotaki, M. Kando, H. Dewa, S. Kondo, Y. Shibata, K. Ishi, M. Ikezawa, Nucl. Instrum. and Meth. A 410 (1998) 424.
[19] T. Watanabe, J. Sugahara, K. Yoshii, M. Uesaka, T. Ueda, Y. Shibata, in: Proceedings of the Sixth European Particle Accelerator Conference, Stockholm, Sweden, 22–26 June 1998, IOP, Bristol, 1998, p. 1632.
[20] X.J. Wang, M. Babzien, K. Batchelor, I. Ben-Zvi, R. Malone, I. Pogorelsky, X. Qiu, J. Sheehan, J. Sharitka, T. Srinivasan-Rao, Nucl. Instrum. and Meth. A 375 (1996) 82.
[21] M. Uesaka, T. Watanabe, T. Ueda, M. Kando, K. Nakajima, H. Kotaki, A. Ogata, J. Nucl. Mater. 248 (1997) 380.
[22] Z. Zuo, Y. Katsumura, K. Ueda, K. Ishigure, J. Chem. Soc. Faraday Trans. 93 (1997) 533.
[23] H. Dewa, H. Ahn, S. Kondoh, H. Kotaki, H. Harano, K. Kinoshita, K. Yoshii, M. Kando, H. Nakanishi, Nucl. Instrum. and Meth. A 410 (1998) 357.
[24] K. Kotaki, K. Nakajima, M. Kando, H. Dewa, S. Kondo, F. Sakai, T. Watanabe, T. Ueda, H. Nakanishi, K. Yoshii, A. Ogata, K. Kinoshita, M. Uesaka, in: Proceedings of the Sixth International Conference on X-ray Lasers, Kyoto, Japan, 31 August–4 September 1998, Inst. Phys. Conf. Ser. No. 159, IOP, Bristol, 1999, p. 565.
[25] A. Takeshita, M. Uesaka, T. Watanabe, M. Yamamoto, N. Kaneko, Nucl. Instrum. and Meth. A 421 (1999) 43.
[26] W.R. Nelson, H. Hirayama, D.W.O. Rogers, The EGS4 Code System, SLAC-265, Stanford University, Stanford, 1985.
[27] G.F. Knoll, Radiation Detection and Measurement, 2nd Ed., Wiley, New York, 1979, p. 30 (Chapter 2).
[28] A.F. Bielajew, D.W.O. Rogers, Nucl. Instrum. and Meth. B 18 (1987) 165.
[29] A.F. Bielajew, R. Mohan, C.-S. Chui, Improved Bremsstrahlung Photon Angular Sampling in the EGS4 Code System, PIRS-0203, NRCC, Ottawa, 1989.
[30] Y. Namito, H. Hirayama, Nucl. Instrum. and Meth. A 423 (1999) 238.
[31] E. Casnati, A. Tartari, C. Baraldi, J. Phys. B 15 (1982) 155.
[32] S.T. Manson, D.J. Kennedy, At. Data Nucl. Data Tables 14 (1974) 111.